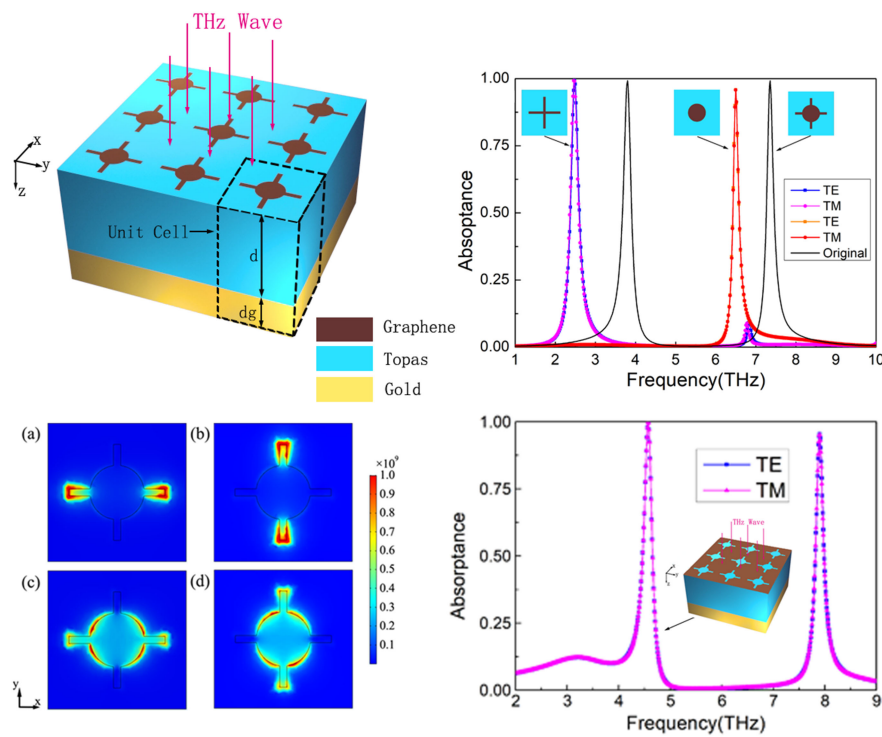


# Tunable Terahertz Perfect-Absorbers With Dual Peak Based on Reverse Graphene Patch Metamaterials

Volume 13, Number 3, June 2021

Yifan Chen  
Xusheng Pan  
Zhiyu Bao  
Yiqing Wang  
Zheng-Da Hu  
Jicheng Wang



DOI: 10.1109/JPHOT.2021.3075466

# Tunable Terahertz Perfect-Absorbers With Dual Peak Based on Reverse Graphene Patch Metamaterials

Yifan Chen,<sup>1</sup> Xusheng Pan,<sup>1</sup> Zhiyu Bao,<sup>1</sup> Yiqing Wang,<sup>1</sup>  
Zheng-Da Hu<sup>1,2</sup>, and Jicheng Wang<sup>1,2</sup>

<sup>1</sup>School of Science, Jiangsu Provincial Research Center of Light Industrial Optoelectronic Engineering and Technology, Jiangnan University, Wuxi 214122, China

<sup>2</sup>State Key Laboratory of Applied Optics, Changchun Institute of Optics, Fine Mechanics and Physics, Chinese Academy of Sciences, Changchun 130033, China

DOI:10.1109/JPHOT.2021.3075466

This work is licensed under a Creative Commons Attribution 4.0 License. For more information, see <https://creativecommons.org/licenses/by/4.0/>

Manuscript received March 30, 2021; revised April 19, 2021; accepted April 21, 2021. Date of publication April 28, 2021; date of current version May 7, 2021. This work was supported in part by the National Natural Science Foundation of China under Grant 11811530052, in part by the Inter-governmental Science and Technology Regular Meeting Exchange Project of Ministry of Science and Technology of China under Grant CB02-20, in part by the Open Fund of State Key Laboratory of Applied Optics under Grant SKLAO2020001A04, and in part by the Undergraduate Research and Innovation Projects of Jiangnan University under Grant 2020366Y. Corresponding author: Jicheng Wang (e-mail: jcwang@jiangnan.edu.cn).

**Abstract:** In this paper, we proposed a tunable graphene-based metamaterial absorber (MA) at dual terahertz band to achieve perfect absorption. The electric field intensity distributions of demonstrated structure is illustrated to explain the origin of two absorption peaks. Simulation result shows the proposed MA owning polarization-insensitive property and wide incident angle tolerance. An inversion algorithm is used to extract the equivalent impedance and explore the physical mechanism of multiple-peak absorption. The equivalent impedance is explored through algorithm when the Fermi energy level alters, consequently the variation of resonant frequency of corresponding absorption peak is determined. Simultaneously, the resonant frequencies of absorption peaks can be adjusted by changing the geometric parameters of the graphene. Furthermore, we adapt the proposed structure into reversely designed pattern, achieving similar characteristic of dual-band absorption peaks and tunability. Thus, our work provides new insight and useful design guidance to various tunable multiple band terahertz metamaterial perfect-absorbers.

**Index Terms:** Perfect absorber, inversion algorithm, reverse pattern, graphene-based metamaterial, terahertz.

## 1. Introduction

Metamaterials, burgeoning artificial materials which are composed of subwavelength unit cells, have engaged many scientists' interests because of its special properties which differ from usual natural materials. It can achieve negative permittivity by periodic metal-dielectric arrays [1]–[3]. As one of promising applications, metamaterial absorbers (MA) had attracted considerable numbers of researchers to pay their attention on it, ascribing to its marvellous performance and convenient tunability, and absorbers within the terahertz (THz) radiation frequency range are in high demand. Terahertz radiation frequency domain ranges from 0.1 to 10 THz, and it has extensive applications in many fields such as imaging, sensing, communications and detection [4]–[7]. Since the primary

theoretical and experimental demonstration metamaterial absorber (MA) was achieved by Landy et al. in 2008 [8], [9], numerous MAs had been designed with different metamaterials and structures. One of the most important features of MAs is that its operating frequencies can be tuned by modifying the geometric or material parameters, which makes MAs widely applied in various actual devices such as sensors [10], filters [11], switch [12], solar photovoltaic devices [13] and so on. Recently, researchers had made great efforts to obtain multi-band or broadband MAs [14]–[17], simultaneously try to achieve perfect absorption [18]–[20]. Among those metamaterials, graphene as a two-dimensional hexagonal grid of carbon atoms, has gained lots of attention owing to its unique chemical and optical properties. By adjusting the bias voltage, the Fermi energy of graphene could be easily changed [21], [22], and that feature makes graphene-based metamaterial the most potential material to fabricate the tunable MA compared with other metamaterials. Moreover, graphene has a wide absorption frequency domain which could range from THz to microwave regions [23], [24]. Therefore, many graphene-based MAs which operate in THz range had been demonstrated and simulated in recent years.

Being Inspired by those previous works, we propose a graphene-based tunable dual-band terahertz metamaterial absorber that achieves perfect absorption in this paper. It's composed of a polyethylene cyclic olefin copolymer (Topas) dielectric layer with monolayer graphene on the top surface and a base structure using gold as a ground plane that reflects electromagnetic waves. Graphene on the surface is designed in shape of a cross, overlapping a circle at its center. The proposed structure is simulated by the commercial finite element method (FEM) in order to acquire precise result of perfect absorption peaks. As a consequence, two absorption peaks with the both absorption rate higher than 99.26% are demonstrated, and the resonant frequencies locate at 3.81THz and 7.36THz respectively. The frequencies of two absorption peaks can be regulated by changing the geometry parameters or the chemical potential of the graphene, simultaneously the proposed structure gives polarization-insensitive performance and wide incident angle tolerance. We present theoretical results by using the updated inverse parameter extraction method with certain parameters in order to have a better understanding of the inherent regularity of the multiple absorption peaks, and the theoretical computing results are accurately coincide with the simulation data. To further extend the model, we also simulated the reversely designed pattern of the graphene on the surface. Comparing with the proposed graphene structure, the similar multiple absorption peaks and features of tunability are explored under the reversely designed pattern, and these characteristics make the coincidence of the resonant frequencies of reversely designed pattern and original one possible.

## 2. Design of the Absorber and Simulation Results

As Fig. 1(a) illustrates the three-dimensional structure of the graphene-based absorber, the main body of the proposed structure is made by two parts: blue layer with thickness of  $d$  represents a dielectric layer made by Topas which has a relative permittivity of 2.35 [25], and yellow layer with thickness of  $dg$  stands for substrate using gold as full reflection substrate. Brown part lying on the upper surface of the dielectric layer Topas represents the graphene strip, and the thickness of monolayer graphene is about 0.34 nm. Thus, the graphene on the top surface can be regarded as two-dimensional surface with isotropic surface conductivity. The two-dimensional structure of graphene strip and its geometric parameters is shown in Fig. 1(b). The whole structure can be divided into completely same unit cells which are placed as periodic array. Viewing from the top of the unit cell, it's in a square shape with the length of periodicity  $P$ . Two same rectangle graphene strips with length  $l$  and width  $w$  are placed orthogonally like a cross at the center of the square, overlapping a circle graphene strip with radius  $R$ . The incident THz wave is indicated in the figure as well, as it propagates along Z axis in the incident XZ plane, and the whole structure is investigated under periodic boundary conditions in the x-axis and y-axis directions. Therefore, the normal transverse electric (TE) can be considered as electric field along the x axis and the transverse magnetic (TM) can be regarded as electric field along the y axis. A possible fabrication processes is provided as follows: First, gold is evaporated onto one sides of the Topas by electron

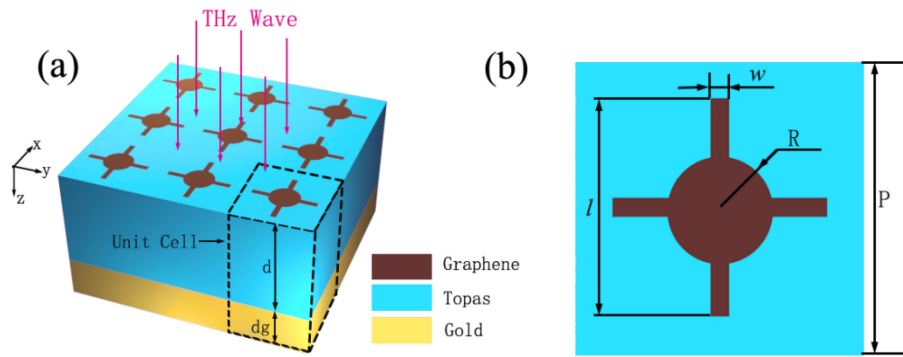


Fig. 1. (a-b)The Schematic of the proposed MA structure. (a) The three-dimensional structure of the proposed graphene-based tunable dual-band terahertz metamaterial absorber. (b) The top view of the unit cell and the detail parameters of graphenestrip. The Parameters here are set as:  $P=4.6\mu\text{m}$ ,  $d=18\mu\text{m}$ ,  $dg=1\mu\text{m}$ ,  $w=0.24\mu\text{m}$ ,  $R=0.9\mu\text{m}$ ,  $l=1.6\mu\text{m}$ .

beam evaporation. Then, a large scale graphene sheet grown on copper can be transferred on the Topas layer by the wet transfer technique. At last, the graphene pattern is defined and the redundant region is removed by using oxygen plasma and electron-beam lithography (EBL).

The graphene on the surface can be simulated by setting the surface current density, as the surface conductivity of graphene can be acquired from Kubo formula [26]–[28]:

$$\sigma(\omega)_{\text{gra}} = \sigma(\omega)_{\text{inter}} + \sigma(\omega)_{\text{intra}} = \frac{2e^2k_B T}{\pi\hbar^2} \frac{i}{\omega + i/\tau} \ln \left[ 2 \cosh \left( \frac{E_f}{2k_B T} \right) \right] + \frac{e^2}{4\hbar^2} \left[ \frac{\frac{1}{2} + \frac{1}{\pi} \arctan \left( \frac{\hbar\omega - 2E_f}{2k_B T} \right)}{-\frac{i}{2\pi} \ln \frac{(\hbar\omega + 2E_f)^2}{(\hbar\omega - 2E_f)^2 + 4(k_B T)^2}} \right] \quad (1)$$

Where  $\sigma(\omega)_{\text{inter}}$  and  $\sigma(\omega)_{\text{intra}}$  are the interband and intraband transition contributions of the graphene, and  $k_B$ ,  $\hbar$ ,  $e$  represent the Boltzmann constant, reduced Plank constant, electron charge respectively.  $\omega$  is the angular frequency of the incident terahertz wave,  $E_f$  is the Fermi energy level of graphene,  $\tau$  is the electron-phonon relaxation time, and  $T$  represents the ambient temperature of Kelvin. As the operating frequency of the proposed MA locates mainly in THz range and the MA works at room temperature ( $T = 300\text{K}$ ), the condition  $E_f \gg \hbar\omega$  and  $E_f \gg k_B T$  is fulfilled. Consequently, the Kubo formula can be simplified to a Drude-like equation [29]–[31]:

$$\sigma(\omega)_{\text{gra}} = \frac{e^2 E_f}{\pi \hbar^2} \frac{i}{(\omega + i/\tau)} \quad (2)$$

Where the  $\tau = \mu E_f / (ev_2 F)$ ,  $E_f$  is set to 0.5 eV,  $v_f$  denotes the graphene Fermi velocity with the value of  $1 \times 10^6 \text{m}\cdot\text{s}^{-1}$ , and  $\mu = 30000 \text{cm}^2\text{V}^{-1}\text{S}^{-1}$  is the media carrier mobility [32].

The absorptance spectrum of the proposed absorber under normal transverse electric (TE) and transverse magnetic (TM) polarized incident wave is shown in Fig. 2(a). The resonant frequencies of the absorber are identical under TE and TM polarized incident wave, with the first absorption peak locating at 3.80 THz and the second absorption peak locating at 7.36 THz. To further investigate the emergence of dual absorption peak, we divide the original shape of graphene into two individual parts and study their absorption properties respectively. Fig. 2(b) shows the result of each individual part. Single resonant frequency of circle-shape graphene locates at 6.50 THz, while the cross-shape graphene emerge with double resonant frequencies at 2.48 THz and 6.84 THz. Besides, and both parts give identical resonant frequency under TE and TM polarized incident wave. When these two individual parts merged, the circle part enhances the absorption of the second resonant frequency of the cross part, simultaneously the new structure resonate with new frequencies.

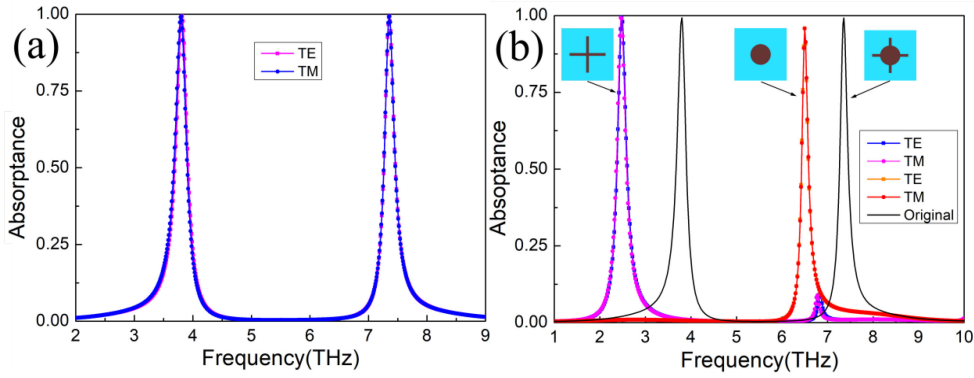


Fig. 2. (a) The simulated absorptance spectra for the MA in Fig. 1 under normal TE and TM polarized incident waves. (b) Absorptance spectra for individual parts under TE and TM incident waves.

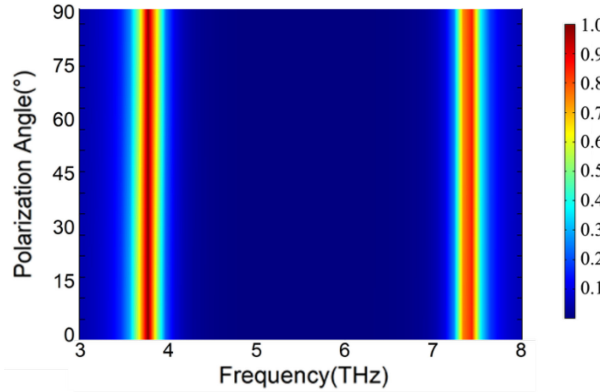


Fig. 3. The absorption spectra of varied polarization angles.

Fig. 3 give further extension of the absorption variation when the polarization incidence angle changes, and it illustrates that the proposed MA gives polarization-insensitive performance. As the pattern of graphene on the top surface is centrosymmetric, the absorptance spectra remain unchanged when the polarization angle of the incident wave alters.

To better illustrate how individual parts influence the absorption of the proposed structure and why the proposed structure is polarization-insensitive, the electric field intensity distributions ( $|E|$ ) under TE and TM incidence are depicted in Fig. 4 at 3.80 THz and 7.36 THz, respectively. For the first absorption peak at 3.80 THz under TE incidence, the localized surface plasmon resonance is induced and mainly restricted surrounding the edge of horizontal rectangle graphene strip as shown in Fig. 4(a). While in Fig. 4(b), under TM incidence at 3.80 THz, the localized surface plasmon resonance is mainly induced around the edge of vertical rectangle graphene strip. Fig. 4(c) and (d) show the electric field intensity at 7.36 THz under TE and TM incidence, respectively. At 7.36 THz, the localized surface plasmon resonance is mostly concentrated at the edge of circle part graphene strip, along with a little contribution from the edge of rectangle part. Comparing the electric field intensity distributions under TE and TM incidence at 7.36 THz. Actually, the electric field intensity distribution under TM incidence can be considered as the 90° rotation of distribution under TE incidence. Thus, when the polarization angle of incident wave changes as Fig. 3 shown, the electric field intensity distribution is actually the rotation of same angle, and it explains the cause of polarization-insensitive performance.

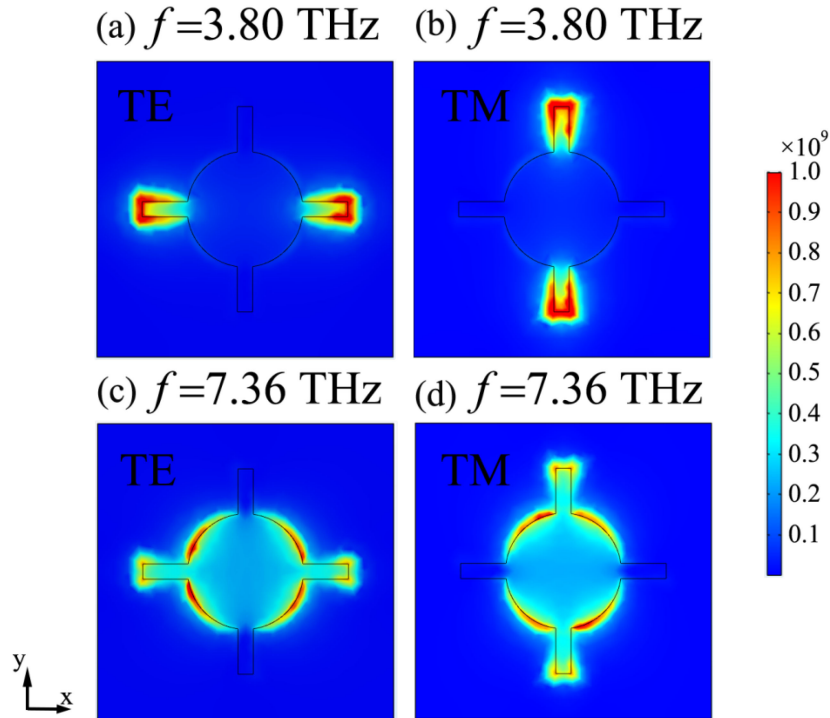


Fig. 4. (a-d) The electric field intensity distributions ( $|E|$ ) of proposed MA from the top view of the unit cell. At 3.80 THz: (a) TE incidence (b) TM incidence. At 7.36 THz: (c) TE incidence (d) TM incidence.

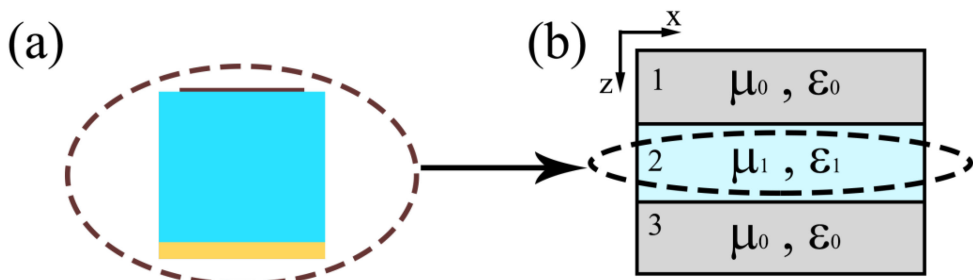


Fig. 5. (a) Lateral view of the unit cell of MA. (b) The equivalent theoretical analysis model of MA. Gray parts represent surrounding outer layers, while the light blue part stands for uniform layer simplified from MA.

### 3. Theoretical Analysis

To give further explanation about the physical mechanism of the phenomenon, an inversion algorithm is applied to extract the normalized impedance of the multiple-peak absorber. The proposed MA can be regarded as a uniform layer with magnetoconductivity  $\mu_1$  and permittivity  $\varepsilon_1$ , and it's surrounded by outer layer, as shown in Fig. 5(b).

Considering the common working condition of the MA, the outer layer is set as air, with magnetoconductivity  $\mu_0$  and permittivity  $\varepsilon_0$ . The THz incident wave which propagates along the Z-axis is reckoned in the model. Therefore, the electromagnetic field strength in any conductive medium can

be expressed as [33]:

$$\begin{cases} E_x = E_{x0} \cdot e^{-jkz} \\ E_y = \frac{k}{\mu\omega} \cdot E_{x0} \cdot e^{-jkz} \end{cases} \quad (3)$$

We set the primary incident wave to be TM polarized, with amplitude  $E_{x0} = 1$ . Consequently, when TM wave propagates in layer 1, the electromagnetic field strength can be written as:

$$\begin{cases} E_{x1} = e^{-jk_1 z} + \Gamma_1 e^{jk_1 z} \\ E_{y1} = \frac{k_1}{\omega\mu_0} e^{-jk_1 x} - \Gamma_1 e^{jk_1 z} \end{cases} \quad (4)$$

Then the TM wave propagates through the interface of the layer 1 and layer 2, the electromagnetic field strength in layer 2 can be written as:

$$\begin{cases} E_{x2} = \tau_1 e^{-jk_2 z} + \tau_1 \Gamma_2 e^{jk_2 z} \\ E_{y2} = \frac{k_2}{\omega\mu_1} (\tau_1 e^{-jk_2 x} - \tau_1 \Gamma_2 e^{jk_2 z}) \end{cases} \quad (5)$$

At last, when TM wave enters the layer 3, the electromagnetic field strength can be written as:

$$\begin{cases} E_{x3} = \tau_1 \tau_2 e^{-jk_3 z} \\ E_{y3} = \frac{k_3}{\omega\mu_0} \tau_1 \tau_2 e^{-jk_3 z} \end{cases} \quad (6)$$

Where  $k_1 = k_3 = k_0$  is the wave number in vacuum,  $k_2 = nk_0$  is the wave number in the relative medium.  $\Gamma_1$  and  $\tau_1$  represent the reflection and transmission coefficients respectively, between layer 1 and layer 2. While  $\Gamma_2$  and  $\tau_2$  stand for the reflection and transmission coefficients between layer 2 and layer 3.

We set the interface of layer 1 and layer 2 to be the X-Y plane, that means  $Z = 0$ . According to the boundary conditions encountered by the electromagnetic wave at the discontinuous interface where  $Z = 0$ , we can obtain:

$$\begin{cases} E_{x1} = E_{x2} \\ E_{y1} = E_{y2} \end{cases} \Rightarrow \begin{cases} 1 + \Gamma_1 = \tau_1 + \tau_1 \Gamma_2 \\ k_1 (1 - \Gamma_1) = \frac{k_2}{\mu_r} (\tau_1 - \tau_1 \Gamma_2) \end{cases} \quad (7)$$

And because the thickness of layer 2 is  $d$ , the Z coordinate of the interface between layer 2 and layer 3 is  $d$ . Therefore, we get:

$$\begin{cases} E_{x2} = E_{x3} \\ E_{y2} = E_{y3} \end{cases} \Rightarrow \begin{cases} \tau_1 e^{-jk_2 d} + \tau_1 \Gamma_2 e^{jk_2 d} = \tau_1 \tau_2 e^{-jk_3 d} \\ \frac{k_2}{\mu_r} (\tau_1 e^{-jk_2 d} - \tau_1 \Gamma_2 e^{jk_2 d}) = k_3 \tau_1 \tau_2 e^{-jk_3 d} \end{cases} \quad (8)$$

Taking all the conditions above into consideration, the scattering parameters can be expressed as:

$$\begin{cases} S_{11} = \frac{\Gamma_1 (1 - (e^{-jk_2 d})^2)}{1 - (\Gamma_1 e^{-jk_2 d})^2} \\ S_{21} = \frac{1 - \Gamma_1^2}{1 - (\Gamma_1 e^{-jk_2 d})^2} e^{-jk_2 d} \end{cases} \quad (9)$$

Where  $\Gamma_1 = (Z-1)/(Z+1)$ . Besides,  $S_{21} = 0$  because we use gold as a full reflection plane in the structure of MA. Basing on the selection of sign [34], [35], We finally obtain:

$$Z = \pm \sqrt{\frac{(1 + S_{11})^2 - S_{21}^2}{(1 - S_{11})^2 - S_{21}^2}} = \frac{1 + S_{11}}{1 - S_{11}} \quad (10)$$

To maximize the absorption of proposed MA, the reflection should be minimum. Which means, the normalized impedance of proposed MA should be close enough to the impedance of free space. Closer the real part of the normalized impedance to unity and the imaginary part to vanishing, greater the absorptance of structure could be.

To give intuitive expression of the relation between the normalized impedance and absorptance, the mathematical consequence of normalized impedance and simulation result of absorptance

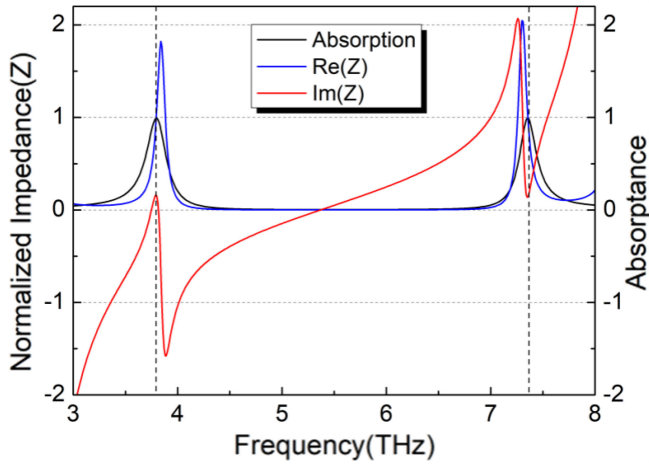


Fig. 6. Normalized impedance obtained by inversion algorithm and absorptance curve.

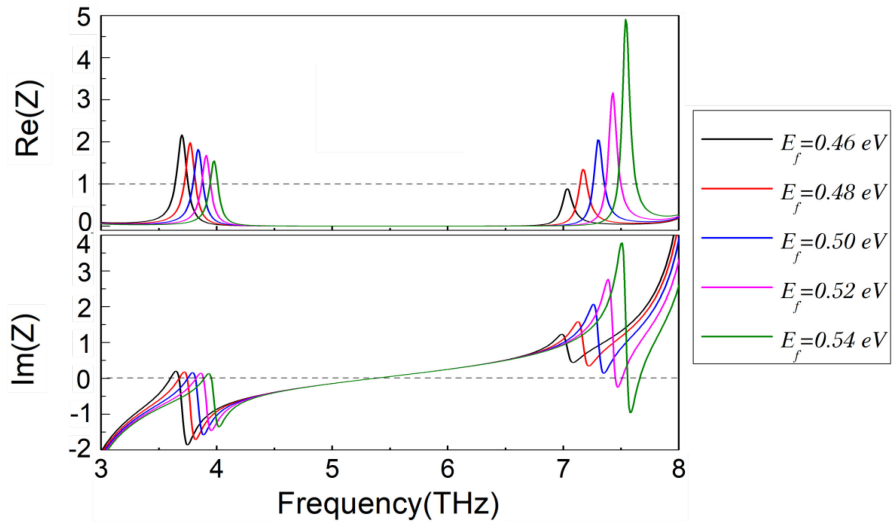


Fig. 7. Variation of normalized impedance when Fermi energy level changes.

are both depicted in Fig. 6. Both resonant absorption peaks coincide at the frequency where the real part of the normalized impedance approaches 1. The value of normalized impedance are  $1.0892+0.1524j$  and  $0.9359+0.1529j$ , at 3.80 THz and 7.36 THz respectively. The exploration of normalized impedance is vital when optimize the structure of the MA and figure out potential absorption peaks. The normalized impedance varies when the Fermi energy level of the graphene changes, and use the relation between normalized impedance and absorption peaks, the resonant frequency of absorption peak can be predicted with different values of Fermi energy levels.

As shown in Fig. 7, the resonant frequencies of real part and the imaginary part of normalized impedance appear blue shifted when the Fermi energy level increasing, simultaneously the maximum value of real part which corresponding to the second absorption peak raises rapidly. Using the theoretical analysis we had proved above, two lines are drawn at where the real part of normalized impedance values one and the image part values zero , to indicate the potential locations of absorption peaks when the Fermi energy level varies. Therefore, we predict that the resonant frequency of the absorption peak would also appear blue shifted when the Fermi energy

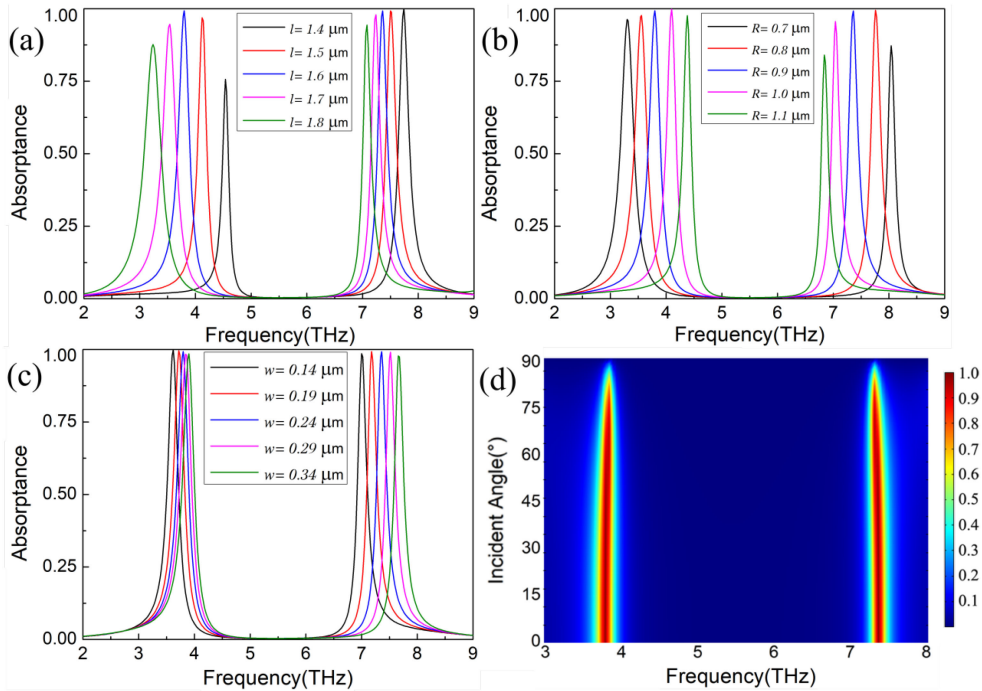


Fig. 8. (a–c) The absorptance spectra variation analysis by changing  $l$ ,  $R$  and  $w$ , respectively. (d) The absorptance spectra variation analysis by changing incident angle. Only single parameter changes and others are set as default.

level increases, and the altered frequencies are determined according to the theoretical analysis. The prediction is confirmed in the next section with further explanation and more details.

#### 4. Absorptance Variation Analysis

The resonant frequencies of dual absorption peaks can be changed by adjusting the geometric parameters of graphene on the top surface of MA. The changed absorptance spectra are illustrated in Fig. 8, with variation of geometric parameters and incident angle.

Fig. 8(a) shows the variation of absorptance curve when  $l$  changes. As  $l$  increasing from  $1.4 \mu\text{m}$  to  $1.8 \mu\text{m}$ , both two absorption peaks appears red-shifted, The first resonant frequency varies from  $4.54 \text{ THz}$  to  $3.24 \text{ THz}$ , with the absorptance value floating from  $0.756$  to  $0.993$ . While the second resonant frequency changes slightly form  $7.08 \text{ THz}$  to  $7.74 \text{ THz}$  when  $l$  increasing, and the absorptance value drops marginally from  $0.999$  to  $0.943$ . However, the absorption peaks change in a different way when  $R$  alters. As shown in Fig. 8(b), when  $R$  varying form  $0.7 \mu\text{m}$  to  $1.1 \mu\text{m}$ , the first resonant frequency appears blue-shifted while the second resonant frequency appears red-shifted. Compare to Fig. 8(a), the variation of absorptance value mainly happens on the second resonant frequency which floating from  $0.840$  to  $0.993$ , while absorptance value of the first resonant frequency changes a little. Fig. 8(c) shows the alteration of absorptance spectra when the parameter  $w$  increasing. Both two resonant frequencies appears blue-shifted, but the variation of second absorption peak is greater than the first absorption peak, while the absorptance values are almost unchanged. From the electric field intensity distribution illustrated in Fig. 4 and the exploration mentioned above, the relationship between geometric changing and absorptance variation could be explained. The emergence of first absorption peak is mainly caused by the cross part while the second absorption peak is caused by circle part. Thus, when the parameter  $l$  of rectangle graphene strip's length changes, the variation would mainly act on the absorption

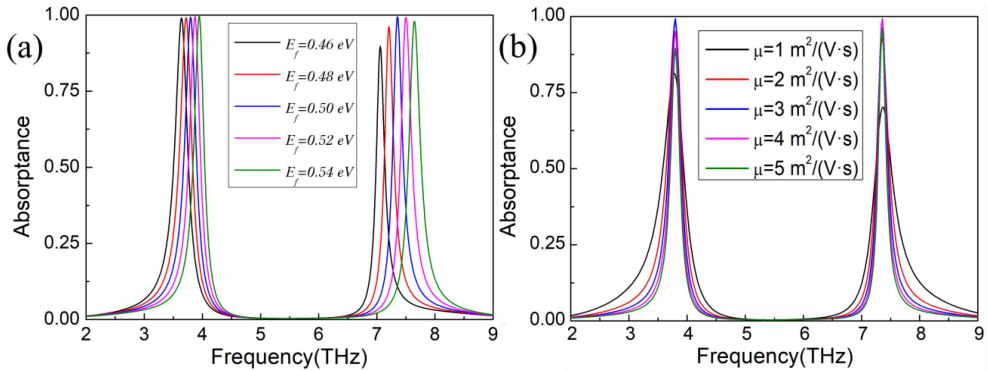


Fig. 9. (a) Fermi energy level variation analysis. (b) The carry mobility variation analysis.

peak corresponding to the rectangle part, which is the first absorption peak. However, because the circle part has the function of enhancing another slight absorption peak caused by cross part, it also influence the resonant frequency of cross part when the parameter  $R$  of circle graphene part's radius changes. As the value of  $R$  keeps raising, the cross part of graphene would finally merge with circle part, and the whole structure remains a circle graphene pattern. From the view of absorptance spectra, two absorption peaks would combine into single peak as  $R$  increasing. The absorption spectra are depicted in Fig. 8 (d) when the angle of incident wave changes. The proposed MA shows a wide incident angle tolerance, when the incident angle scanning form  $0^\circ$  to  $70^\circ$ , the absorption spectra is almost unchanged. As incident angle increasing from  $70^\circ$  to  $90^\circ$ , the absorption peak gradually vanish.

Excepting for changing the geometric parameters, the absorption vary when the chemical potential of graphene alters as well. Fig. 9(a) depicts the variation of absorptance spectra when changing the Fermi energy level of the graphene. In the previous section, we use the inversion algorithm to analyse the normalized impedance and predicted that when Fermi energy level increases, the resonant frequencies would perform blue-shifted. The simulation data coincide exactly with the theoretical prediction, as the first resonant frequency varies from 3.64 THz to 3.94 THz while the second varies from 7.06 THz to 7.65 THz. The absorptance spectra variation caused by changing the carry mobility is shown in Fig. 9(b) as well. As the value of carry mobility  $\mu$  increase from 10000 to 30000, absorptance value of two peaks both raise. But when  $\mu$  increasing from 30000 to 50000, both absorption peaks starts to decline and the first peak dropping faster than the second one. Thus, only when  $\mu$  is around  $30000 \text{ cm}^2 \text{ V}^{-1} \text{ S}^{-1}$  does the proposed structure achieve perfect absorption.

Moreover, we explore the reversely designed pattern of the graphene strip on the top surface of proposed MA [36], and the structure is shown in Fig. 10(a) and (b). In comparison with original structure shown in Fig. 1, now the entire top surface is covered with graphene, while the place which used to cover with graphene strip is hollowed.

As shown in Fig. 11(a), the simulation result of the reversely designed pattern gives dual-band absorption peak and polarization-insensitive performance which is similar to the characteristics of original pattern. Simultaneously, two resonant frequencies give relatively high absorptance which values of 0.997 at 4.57 THz and 0.954 at 7.90 THz respectively. Because the graphene placement of reverse pattern differ from the initial proposed pattern, the resonant frequencies would certainly display discrepancy between two structures.

The electric field intensity distributions ( $|E|$ ) under TE and TM incidence are shown in Fig. 11 at two absorption peaks respectively. As we obtain the regularity from Fig. 4 that the localized surface plasmon resonance is mainly restricted surrounding the edge of graphene, it's the same for the reversely designed pattern. However, since the graphene becomes the reversely designed pattern,

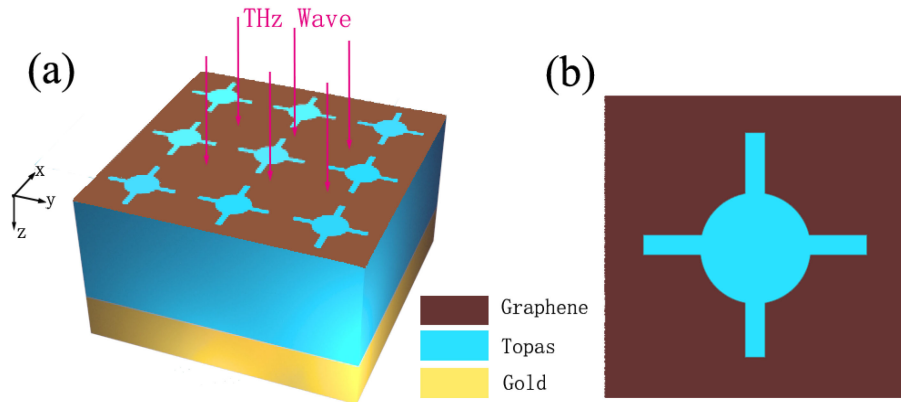


Fig. 10. (a–b) The reversely designed structure of the proposed MA. (a) The three-dimensional structure of reversely designed structure. (b) The top view of the unit cell of the reversely designed pattern. All the detail parameters are set as default.

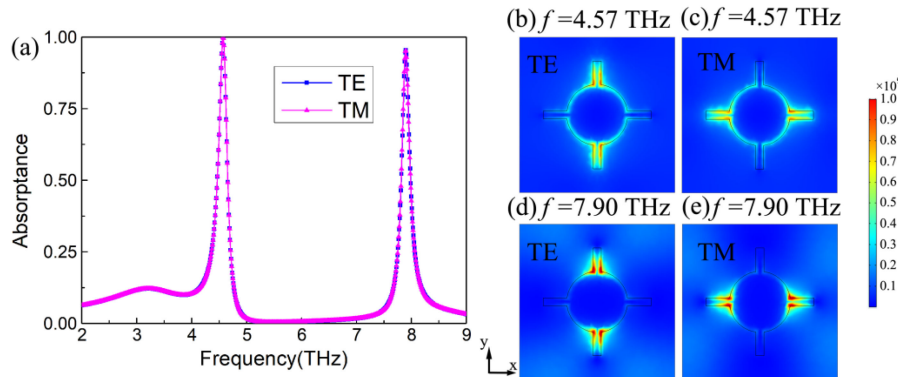


Fig. 11. (a) Absorptance spectra of reversely designed pattern. (b–e) The electric field intensity distributions of the reversely designed pattern from the top view of the unit cell. At 4.57 THz: (a) TE incidence (b) TM incidence; At 7.90 THz: (c) TE incidence (d) TM incidence.

the existence of graphene at the edge becomes inverse as well. Fig. 11(b) and (c) shows the first absorption peak at 4.57 THz under TE and TM polarization incidence, respectively. Comparing with Fig. 4, the hollow in the graphene of reversely designed pattern cause the discontinuity in the electric field intensity distribution between bilateral graphene edges. Under TE incidence at 4.57 THz, the localized surface plasmon resonance is almost equally distributed around the vertical rectilinear edge and the curvy edge of graphene, as illustrated in Fig. 11(b). The electric field intensity distribution under TM incidence can be acquired by rotating 90° from the figure of TE incidence, and this peculiarity resemble the original structure. Fig. 11(d) and (e) depicts the second absorption peak at 7.90 THz under TE and TM polarization incidence respectively, and the localized surface plasmon resonance is restricted mainly at the intersection of rectilinear edge and the curve edge. From the exploration about the proposed MA above, similar tunability on geometric variation and Fermi energy level alteration can be ascertained. Thus, the resonant frequencies of the reversely designed pattern can be precisely regulated to coincide the resonant frequencies of original pattern, and Fig. 12 illustrates the result of adjustment. Although the frequency location of absorption peaks is accurately corresponded, the value of absorptance would be partly sacrificed due to the parameters' variation. From Fig. 9(b) we know altering the carrier mobility  $\mu$  can regulate the absorptance value without changing the frequencies location of absorption peaks. As

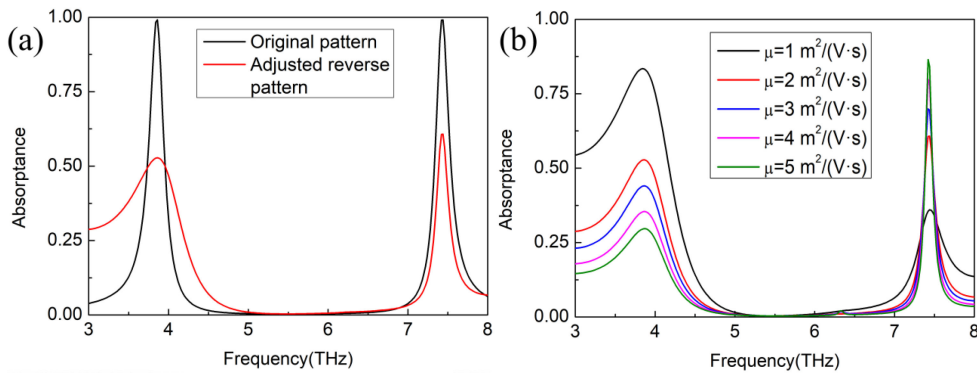


Fig. 12. (a) The absorptance spectra of original pattern and adjusted reversely designed pattern. The parameters of adjusted reverse pattern are  $E f = 0.45 \text{ eV}$  and  $\mu = 23200 \text{ cm}^2/(\text{V}\cdot\text{s})$ . (b) The absorptance spectra of carry mobility variation under adjusted reverse pattern.

Fig. 12(b) depicts the absorptance spectra of carry mobility variation under the reverse pattern, two absorption peaks present contrary changing tendency when  $\mu$  increasing. Therefore, the adjusted reverse pattern couldn't reach perfect absorption at both absorption peaks. To let the trend of spectra under the regulated structure close to the original pattern, we chose the appropriate  $\mu$  to make the absorptance value of two peaks close.

## 5. Conclusion

In summary, the graphene-based tunable dual-band terahertz metamaterial modulator with perfect absorption has been demonstrated. The absorptance spectra shows polarization-insensitive performance and wide incident angle tolerance. Two absorption peaks can be adjusted to the expected frequencies by altering the geometric parameters and chemical potential of the graphene. The inversion algorithm is carried out to explore the physical mechanism of two absorption peaks by computing the normalized impedance, and further relation between normalized impedance and absorption peak is used to predict the variation of resonant frequency when the Fermi energy level changes. Moreover, we give the reversely designed pattern of the graphene structure, finding the same polarization-insensitive performance and dual absorption peaks, with relatively high absorptance value but shifted resonant frequencies. Similar features of absorptance spectra variation by changing geometric parameters and chemical potential are unveiled, which give us the access to regulating the resonant frequencies of original pattern and reversely designed pattern coincided. Therefore, this work provides useful solution and perspective in tunable high-performance multi-band terahertz absorber design.

## References

- [1] V. Shalaev *et al.*, "Optical negative-index metamaterials," *Nature Photon.*, vol. 1, pp. 41–48, Jan. 2007.
- [2] X. Xing *et al.*, "Terahertz metamaterial beam splitters based on untraditional coding scheme," *Opt. Exp.*, vol. 27, no. 20, pp. A1627–A1635, Sep. 2019.
- [3] S. Liu *et al.*, "A broadband terahertz absorber using multi-layer stacked bars," *Appl. Phys. Lett.*, vol. 106, no. 15, Apr. 2015, Art. no. 151601.
- [4] M. Tonouchi, "Cutting-edge terahertz technology," *Nature Photon.*, vol. 1, no. 2, pp. 97–105, Jan. 2007.
- [5] P. H. Siegel, "Terahertz technology," *IEEE Trans. Microw. Theory Techn.*, vol. 50, no. 3, pp. 910–928, Mar. 2002.
- [6] H. T. Chen *et al.*, "Terahertz imaging with nanometer resolution," *Appl. Phys. Lett.*, vol. 83, no. 15, pp. 3009–3011, Oct. 2003.
- [7] H.-J. Song, and T. Nagatsuma, "Present and future of terahertz communications," *IEEE Trans. THz Sci. Techn.*, vol. 1, no. 1, pp. 256–263, Oct. 2011.
- [8] N. I. Landy *et al.*, "Perfect metamaterial absorber," *Phys. Rev. Lett.*, vol. 100, no. 20, May 2008, Art. no. 207402.

- [9] H. Tao, N. I. Landy, C. M. Bingham, X. Zhang, R. D. Averitt, and W. J. Padilla, "A metamaterial absorber for the terahertz regime: Design, fabrication and characterization," *Opt. Exp.*, vol. 16, no. 10, pp. 7181–7188, May 2008.
- [10] C. Caucheteur, T. Guo, F. Liu, B. O. Guan, and J. Albert, "Ultrasensitive plasmonic sensing in air using optical fibre spectral combs," *Nature Commun.*, vol. 7, no. 1, Nov. 2016, Art. no. 13371.
- [11] I. J. H. McCrindle, J. Grant, T. D. Drysdale, and D. R. S. Cumming, "Multi-spectral materials: Hybridisation of optical plasmonic filters and a terahertz metamaterial absorber," *Adv. Opt. Mater.*, vol. 2, no. 2, pp. 149–153, Feb. 2014.
- [12] T. Bai *et al.*, "High-performance sensitive TE/TM mode switch with graphene-based metal-dielectric resonances," *IEEE Sensors J.*, vol. 21, no. 3, pp. 2791–2797, Sep. 2021.
- [13] Q. Q. Liang *et al.*, "Numerical study of the meta-nanopyramid array as efficient solar energy absorber," *Opt. Mater. Exp.*, vol. 3, no. 8, pp. 1187–1196, Aug. 2013.
- [14] Z. Bao *et al.*, "Coordinated multi-band angle insensitive selection absorber based on graphene metamaterials," *Opt. Exp.*, vol. 27, no. 22, pp. 31435–31445, Oct. 2019.
- [15] Y. Liu, R. Zhong, J. Huang, Y. Lv, C. Han, and S. G. Liu, "Independently tunable multi-band and ultra-wide-band absorbers based on multilayer metal-graphene metamaterials," *Opt. Exp.*, vol. 27, no. 5, pp. 7393–7404, Mar. 2019.
- [16] H. Li, J. Niu, and G. Wang, "Dual-band, polarization-insensitive metamaterial perfect absorber based on monolayer graphene in the mid-infrared range," *Results Phys.*, vol. 13, May 2019, Art. no. 102313.
- [17] Z. Yi *et al.*, "Nanoribbon-ring cross perfect metamaterial graphene multi-band absorber in THz range and the sensing application," *Results Phys.*, vol. 14, May 2019, Art. no. 102367.
- [18] J. Wang *et al.*, "Perfect absorption and strong magnetic polaritons coupling of graphene-based silicon carbide grating cavity structures," *J. Phys. D*, vol. 52, no. 1, Oct. 2018, Art. no. 015101.
- [19] H. J. Li, C. S. Ji, Y. Z. Ren, J. G. Hu, M. Qin, and L. L. Wang, "Investigation of multiband plasmonic metamaterial perfect absorbers based on graphene ribbons by the phase-coupled method, carbon," *Carbon*, vol. 141, pp. 481–487, Jan. 2019.
- [20] F. Wang, S. Huang, L. Li, W. Chen, and Z. Xie, "Dual-band tunable perfect metamaterial absorber based on graphene," *Appl. Opt.*, vol. 57, pp. 6916–6922, Aug. 2018.
- [21] L. Ju *et al.*, "Graphene plasmonics for tunable terahertz metamaterials," *Nature Nanotechnol.*, vol. 6, no. 10, pp. 630–634, Sep. 2011.
- [22] S. Lee *et al.*, "Switching terahertz waves with gate-controlled active graphene metamaterials," *Nature Mater.*, vol. 11, no. 11, pp. 936–941, Sep. 2012.
- [23] F. Bonaccorso *et al.*, "Graphene photonics and optoelectronics," *Nature Photon.*, vol. 4, no. 9, pp. 611–622, Jun. 2010.
- [24] F. Xia, H. Wang, D. Xiao, M. Dubey, and A. Ramasubramaniam, "Two-dimensional material nanophotonics," *Nature Photon.*, vol. 8, no. 12, pp. 899–907, Oct. 2014.
- [25] K. Xu, J. Li, A. Zhang, and Q. Chen, "Tunable multi-band terahertz absorber using a single-layer square graphene ring structure with T-shaped graphene strips," *Opt. Exp.*, vol. 28, pp. 11482–11492, Mar. 2020.
- [26] E. H. Hwang, and S. D. Sarma, "Dielectric function, screening, and plasmons in two-dimensional grapheme," *Phys. Rev. B*, vol. 75, no. 20, May 2007, Art. no. 205418.
- [27] L. A. Falkovsky, and S. S. Pershoguba, "Optical far-infrared properties of a graphene monolayer and multilayer," *Phys. Rev. B*, vol. 76, Jul. 2007, Art. no. 153410.
- [28] G. W. Hanson, "Dyadic green's functions and guided surface waves for a surface conductivity model of graphene," *J. Appl. Phys.*, Apr. 2008, vol. 103, Art. no. 064302.
- [29] S. Xiao *et al.*, "Tunable light trapping and absorption enhancement with graphene ring arrays," *Phys. Chem. Chem. Phys.*, vol. 18, no. 38, pp. 26661–26669, Oct. 2016.
- [30] S. Jin *et al.*, "Modulation of terahertz radiation from graphene surface plasmon polaritons via surface acoustic wave," *Opt. Exp.*, vol. 27, no. 8, pp. 11137–11151, Apr. 2019.
- [31] J. Zhang, Z. Zhu, W. Liu, X. Yuan, and S. Qin, "Towards photodetection with high efficiency and tunable spectral selectivity: Graphene plasmonics for light trapping and absorption engineering," *Nanoscale*, vol. 7, no. 32, pp. 13530–13536, Jul. 2015.
- [32] J. H. Ge *et al.*, "Tunable dual plasmon-induced transparency based on a monolayer graphene metamaterial and its terahertz sensing performance," *Opt. Exp.*, vol. 28, no. 21, pp. 31781–31795, Oct. 2020.
- [33] M. F. Iskander, *Electromagnetic Fields and Waves*, 2nd ed. Long Grove, IL, USA: Waveland Press, 2013.
- [34] D. R. Smith, S. Schultz, P. Markoš, and C. M. Soukoulis, "Determination of effective permittivity and permeability of metamaterials from reflection and transmission coefficients," *Phys. Rev. B*, vol. 65, no. 19, Nov. 2001, Art. no. 195104.
- [35] D. R. Smith *et al.*, "Electromagnetic parameter retrieval from inhomogeneous metamaterials," *Phys. Rev. E*, vol. 71, Apr. 2005, Art. no. 036617.
- [36] K. Xu, Y. Cai, X. Cao, Y. Guo, Y. Zhang, and Q. Chen, "Multiband terahertz absorbers using T-shaped slot-patterned graphene and its complementary structure," *J. Opt. Soc. Amer. B*, vol. 37, no. 10, pp. 3034–3040, Aug. 2020.